Telecommunications and Radio Engineering, 75 (8):745-756 (2016)

PLASMA-BEAM SUPERHETERODYNE FREE ELECTRON LASER WITH *H*-UBITRON PUMPING AND NON-AXIAL ELECTRON BEAM INJECTION*

A.V. Lysenko♦ & G.A. Alekseyenko

Sumy State University, Rymsʹkoho-Korsakova St, 2, Sumy, 40007, Ukraine

♦Address all correspondence to: A.V. Lysenko, E-mail: lysenko_@ukr.net

The authors suggest a cubic-nonlinear theory of a plasma-beam superheterodyne free electron laser (PBSFEL) with H-ubitron pumping and non-axial injection of electron beam. In this laser, a space-charge wave interacts with a cyclotron wave in terms of parametric resonance. While determining signal wave saturation levels it was revealed that the mode using a slow cyclotron wave had the highest saturation level among all possible operation modes of the PBSFEL with the H-ubitron pumping. The beam injection angle producing the maximum gain in the electromagnetic signal has been determined. It was shown that PBSFELs utilizing the slow cyclotron waves were able to produce a powerful coherent electromagnetic radiation in the millimeter wave range.

KEY WORDS: *superheterodyne free electron laser, plasma-beam instability, parametric resonance*

1. INTRODUCTION

Search for the methods of producing powerful coherent electromagnetic radiation in millimeter wave range is one of the priorities in the EHF electronics of today [1–4]. Devices of this frequency range are strongly sought after in theoretical and applied research: for thermonuclear plasma heating, in accelerators of different kind, in medicine, communications etc. Among various EHF devices, a special attention deserve superheterodyne free electron lasers (SHFEL) due to their extremely strong amplifying ability [1,5–7]. High gain factors of such devises are provided by an additional mechanism of amplifying the longitudinal space-charge electron wave (SCW), which contributes to the three-wave parametric resonance. Such mechanism in a plasma-beam SHFEL (PBSHFEL) is the plasma-beam instability.

Our research is devoted to the amplifying ability of PBSHFEL of an *H*-ubitron type with a helical electron beam, where a cyclotron electromagnetic wave is used as a

*Originally published in *Radiophysics and Electronics*, Vol. 7(21), No 1, 2016, pp. 48–54.

signal wave. PBSHFEL with the *H*-ubitron pumping operating at straight electron beams have been considered in detail [8,9]. It was revealed that such devices are able to generate powerful electromagnetic waves in millimeter wave range. Helical electron beams are supposed to enhance their performance [10–19]. The amplifying properties of an *H*-ubitron-type PBSHFEL with a helical beam in a quadratic approximation were investigated in [20]. The properties of a PBSHFEL with an *H*-ubitron and a helical beam in operation modes requiring an extraordinary electromagnetic wave have been considered in [21] taking into account the cube-nonlinear terms. The operation modes of the same FEL configuration with cyclotron electromagnetic waves have not yet been investigated in the cubic approximation. This is the case when the interaction between an electron beam rotating in the magnetic field and a cyclotron electromagnetic wave is expected to be extremely strong, as in this mode the plasma-beam instability is complemented by that of the cyclotron. Thus, in our paper we will closely examine the amplifying properties of this type of PBSHFEL.

2. MODEL

Shown in Fig. 1 is a functional diagram of PBSHFEL of the *H*-ubitron type with a non-axial electron beam injection. Here, the plasma 1 of the Langmuir frequency ω_p is placed into an external homogeneous magnetic field of the density B_0. A helical relativistic electron beam 2 of the Langmuir frequency ω_b ($\omega_b << \omega_p$) crosses a magnetized plasma medium. The beam velocity vector $\vec{\upsilon}_b$ is directed at the angle β to the density vector of the focusing magnetic field $\vec{B}_0$ (Fig. 1), so that $\tan\beta = \overline{\upsilon}_{b\perp} / \overline{\upsilon}_{bz}$, where $\overline{\upsilon}_{b\perp}$ and $\overline{\upsilon}_{bz}$ are the average transversal and longitudinal components of electrons' velocity. Being exposed to the longitudinal magnetic field, the electrons of the plasma-beam system rotate with the frequency ω_H. Here we assume that $\omega_H << \omega_p$. The reversal magnetic field of the undulator 3 of the period $\Lambda = 2\pi / k_2$ is used as a pump.

A high-frequency electromagnetic wave of the frequency ω_1 and the wave number k_1 is applied to the system input. Due to the resonance interaction between the wave $\{\omega_1, k_1\}$ and the undulator field $\{k_2\}$ a space-charge wave of the frequency ω_3 and the wave number k_3 is excited in the plasma-beam medium. The conditions of the parametric resonance in the considered system have the form:

$$\omega_3 = \omega_1, \; k_3 = k_1 + k_2. \tag{1}$$

It should be noted that this PBSHFEL takes advantage of the superheterodyne amplification. The amplification is achieved due to an additional mechanism possessed by one of the waves contributing to the parametric resonance, namely the plasma-beam

instability in case of PBSHFEL [1,2]. It is known that the plasma-beam instability increments are extremely high [1,2]. Due to the additional amplification mechanism, the total amplification factor of the electromagnetic signal wave in PBSHFEL is high, too. That's why such SHFELs are ahead of other types of free electron lasers in terms of their gain.

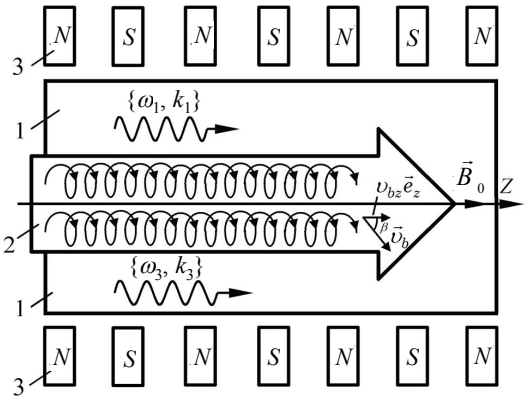

FIG. 1: Functional diagram of PBSHFEL with an H-ubitron and a helical relativistic electron beam

3. BASIC EQUATIONS

We will consider a case when the electron velocity spread and collisions can be neglected. The relativistic quasi-hydrodynamic equation, the continuity equation and the Maxwell equation will be used as the initial ones. The motion equation will be solved by the averaged characteristics method [1,5], and the continuity equation and the field equation – by the slowly-varying amplitude method.

For the SHFEL in question, electric E and magnetic B components of the variable fields of the signal (index 1), pumping (index 2) and SCW (index 3) are written as:

$$\begin{aligned} E_1 &= \left(E_{1x}\vec{e}_x + E_{1y}\vec{e}_y\right)e^{ip_1} + c.c., \\ B_1 &= \left(B_{1x}\vec{e}_x + B_{1y}\vec{e}_y\right)e^{ip_1} + c.c., \\ B_2 &= \left(B_{2x}\vec{e}_x + B_{2y}\vec{e}_y\right)e^{ip_2} + c.c., \\ E_3 &= \left(E_{3z}e^{ip_3} + c.c.\right)\vec{e}_z, \end{aligned} \tag{2}$$

where $p_1 = \omega_1 t - k_1 z$; $p_2 = -k_2 z$; and $p_3 = \omega_3 t - k_3 z$. Thus, the electric and magnetic fields in the working volume of the SHFEL have the form:

$$E = E_1 + E_3, \qquad B = B_1 + B_2 + B_0. \tag{3}$$

While solving the motion equation, we transfer from the quasi-hydrodynamic equation in partial derivatives to its characteristics, the equations in total derivatives, according to the averaged characteristics method [1,5]. The initial motion equations take on the form:

$$\frac{d\upsilon_{qx}}{dt} = \frac{e}{m_e\gamma_q}\left[E_x + \frac{1}{c}\left(\upsilon_{qy}B_z - \upsilon_{qz}B_y\right) - \frac{\upsilon_{qx}}{c^2}\left(\upsilon_{qx}E_x + \upsilon_{qy}E_y + \upsilon_{qz}E_z\right)\right]; \tag{4}$$

$$\frac{d\upsilon_{qy}}{dt} = \frac{e}{m_e\gamma_q}\left[E_y - \frac{1}{c}\left(\upsilon_{qx}B_z - \upsilon_{qz}B_x\right) - \frac{\upsilon_{qy}}{c^2}\left(\upsilon_{qx}E_x + \upsilon_{qy}E_y + \upsilon_{qz}E_z\right)\right]; \tag{5}$$

$$\frac{d\upsilon_{qz}}{dt} = \frac{e}{m_e\gamma_q}\left[E_z + \frac{1}{c}\left(\upsilon_{qx}B_y - \upsilon_{qy}B_x\right) - \frac{\upsilon_{zq}}{c^2}\left(\upsilon_{qx}E_x + \upsilon_{qy}E_y + \upsilon_{qz}E_z\right)\right]; \tag{6}$$

$$\frac{d\gamma_q}{dt} = \frac{e}{m_e\gamma_q}\left[E_x\upsilon_{qx} + E_y\upsilon_{qy} + E_z\upsilon_{qz}\right]. \tag{7}$$

In these equations, υ_{qx}, υ_{qy} and υ_{qz} are components of the velocity vector $\vec{v}_q$ of the beam electrons and plasma (hereinafter the index q takes on the values b and p; index b characterizes the beam parameters, index p is peculiar to the plasma parameters), $\gamma_q = 1/\sqrt{1-(\upsilon_{qx}^2 + \upsilon_{qy}^2 + \upsilon_{qz}^2)/c^2}$ is the relativistic factor, c is the velocity of light, and e and m_e are the charge and mass of electron.

It is also taken into account that, at a non-zero beam injection angle β to the longitudinal focusing magnetic field $\vec{B}_0$, the undisturbed electrons move circumferentially in the transverse plane. Hence, in the motion equations (4)–(7) we substitute:

$$\upsilon_{bx} = \overline{\upsilon}_{b\perp}\cos p_{b0} + \tilde{\upsilon}_{bx},\ \upsilon_{by} = \overline{\upsilon}_{b\perp}\sin p_{b0} + \tilde{\upsilon}_{by},$$

where $\overline{\upsilon}_{b\perp}$ is the undisturbed normal component of the beam velocity vector, p_{b0} is the undisturbed electron rotation phase in the transverse magnetic field, and $\tilde{\upsilon}_{bx}$, $\tilde{\upsilon}_{by}$ are oscillating x- and y-components of the electrons' velocity vector.

The solution of the set (4)–(7) is sought after the method of averaged characteristics [1,5]. The slowly-varying amplitude method is applied to find the variables of electromagnetic fields and concentrations. Finally, we obtain a set of differential equations in a cubic approximation for the x-, y-components of the complex first

harmonic amplitude of the signal wave and the z-component of the first harmonic amplitude of the space-charge wave:

$$\begin{aligned} K_2 \frac{d^2 E_{1x}}{dt^2} + K_1 \frac{dE_{1x}}{dt} + D_1 E_{1x} &= K_3 E_{3z} B_{2x}^* + FX_1, \\ K_2 \frac{d^2 E_{1y}}{dt^2} + K_1 \frac{dE_{1y}}{dt} + D_1 E_{1y} &= K_3 E_{3z} B_{2y}^* + FY_1 , \\ C_2 \frac{d^2 E_{3z}}{dt^2} + C_1 \frac{dE_{3z}}{dt} + D_3 E_{3z} &= C_3 (E_{1x} B_{2y} + E_{1y} B_{2x}) + FZ_3 . \end{aligned} \tag{8}$$

In these equations:

$$\begin{aligned} D_1(\omega_1, k_1) = \frac{i}{c\omega_1} \Bigg\{ k_1^2 c^2 - \omega_1^2 + \sum_q^{b,p} \Bigg[\frac{\omega_q^2}{\overline{\gamma}_q \left(\Omega_{1,q} - \eta_1 \Omega_{q0} \right)^2} \times \\ \times \Bigg(\Omega_{1,q} \left(\Omega_{1,q} - \eta_1 \Omega_{q0} \right) - \frac{\overline{\upsilon}_{q\perp}^2}{2c^2} \left(\omega_1^2 - k_1^2 c^2 \right) \Bigg) \Bigg] \Bigg\} \end{aligned} \tag{9}$$

is the dispersion function of the electromagnetic signal wave,

$$D_3 = \frac{-i\omega_3}{c} \left(1 - \sum_q^{b,p} \frac{\omega_q^2 (1 - \overline{\upsilon}_{qz}^{\,2} / c^2)}{(\omega_3 - k_3 \overline{\upsilon}_{qz})^2 \overline{\gamma}_q} \right) \tag{10}$$

is the dispersion function of the longitudinal SCW, $K_1 = \partial D_1 \big/ \partial (i\omega_1)$; $K_2 = \partial^2 D_1 \big/ 2\partial (i\omega_1)^2$; $C_1 = \partial D_3 \big/ \partial (i\omega_3)$; $C_2 = \partial^2 D_3 \big/ \partial (i\omega_3)^2$; K_3, C_3 are coefficients of the respective differential equations, determined by the frequencies, wave numbers and system parameters, FX_1, FY_1, FZ_3 are functions taking into account the cubic-nonlinear components of the respective equations; $\eta_1 = E_{1y} / (iE_{1x}) = \pm 1$, $\eta_2 = B_{2y} / (iB_{2x}) = \pm 1$ are sign functions (η_1 characterizes the rotation direction of the signal wave's field strength in the longitudinal focusing magnetic field; η_2 characterizes the rotation direction of undulator's spiral magnetic field $\Omega_{0,q} = -\omega_{H,q} / \overline{\gamma}_q$; $\Omega_{1,q} = \omega_1 - k_1 \overline{\upsilon}_{qz}$; $\Omega_{2,q} = -k_2 \overline{\upsilon}_{qz}$; $\Omega_{3,q} = \omega_{3,1} - k_3 \overline{\upsilon}_{qz}$; $\omega_{H,q} = e_q B_0 / (m_e c)$.

The set (8) should be complemented by equations for constant components of velocity and concentration:

$$d\overline{\upsilon}_{\perp q} / dt = V_{\perp q}, \; d\overline{\upsilon}_{zq} / dt = V_{zq}, \; d\overline{n}_q / dt = N_q, \tag{11}$$

where functions $V_{\perp q}$, V_{zq}, N_q allow for the cubic-nonlinear components, depend on the constant components of velocities and concentrations, frequencies, wave numbers and field amplitudes(8), (11) is analyzed by using conventional numerical methods.

In the considered PBSHFEL, the plasma-beam instability acts as a complementary amplification mechanism. In terms of mathematics it means that the dispersion equation for the space-charge wave $D_3(\omega_3, k_3) = 0$ has complex roots. Hence, if we substitute real frequencies and real wave numbers into (10), the dispersion function is not zero ($D_3 \neq 0$). We are able to find the increment of SCW, caused by the plasma-beam instability, by using the third equation of the set (8). While neglecting the parametric resonance (term $C_3 E_{1x} B_{2y}$), the cubic-nonlinear interactions (term FZ_3) and taking into account that $C_2 d^2 E_{3z} / dt^2$, $D_3 E_{3z} >> C_1 dE_{3z} / dt$, it is easy to find, from the derived equation, the growth rate (increment) of the plasma-beam instability $(-D_3 / C_2)^{1/2}$. This is the reason why we include the term $D_3 E_{3z}$ into the equation for SCW.

If a cyclotron wave is used as a signal wave, the system is characterized by the cyclotron instability as well, in which case the dispersion equation for electromagnetic wave $D_1(\omega_1, k_1) = 0$ has complex roots, similarly to that for SCW. Since, if we substitute real frequencies and real wave numbers into (9), the dispersion function of the electromagnetic signal is not zero ($D_1 \neq 0$). The increment of the cyclotron electromagnetic wave can be found by using either the first or the second equations of the set (8). Again, we neglect the parametric resonance (term $K_3 E_{3z,1} B^*_{2x}$ or $K_3 E_{3z,1} B^*_{2y}$), the cubic-nonlinear interactions (term FX_1 or FY_1) , take into account that $K_2 d^2 E_{1x,y} / dt^2, D_1 E_{1x,y} >> K_1 dE_{1x,y} / dt$, and from the derived equation easily find the increment of the plasma-beam instability $(-D_1 / K_2)^{1/2}$. The estimates of the cyclotron instability increment coincide with the reported ones (for example, in [2]).

4. ANALYSIS

The cubic-nonlinear analysis of physical processes occurring in PBSHFEL of the *H*-ubitron type with non-axial electron beam injection will be performed by using conventional numerical methods based on the set (8), (11). The following parameters will be used: the Langmuir plasma frequency $\omega_p = 1 \cdot 10^{12}\ \mathrm{s}^{-1}$, the Langmuir beam frequency $\omega_b = 3 \cdot 10^{10}\ \mathrm{s}^{-1}$, the cyclotron frequency $\omega_H = -5 \cdot 10^{10}\ \mathrm{s}^{-1}$, the energy of electrons in the relativistic beam of 0.51 MeV, the amplitude of the magnetic pumping field density $B_2 = \sqrt{|B_{2x}|^2 + |B_{2y}|^2} = 100$ G.

According to [8], a PBSHFEL of the *H*-ubitron type with an axial injection of electrons has four modes of parametric interaction between the electromagnetic signal wave, *H*-ubitron pumping field and the SCW. The four interaction modes are observed also in case of a non-axial beam injection. The investigation of resonance wave interaction in the PBSHFEL was started by plotting a graph to show how the signal wave and SCW frequencies depend on the wave number, with the beam injection angle to the longitudinal magnetic field being $\beta = 20°$, by using the formulae (9)–(10) (Fig. 2).

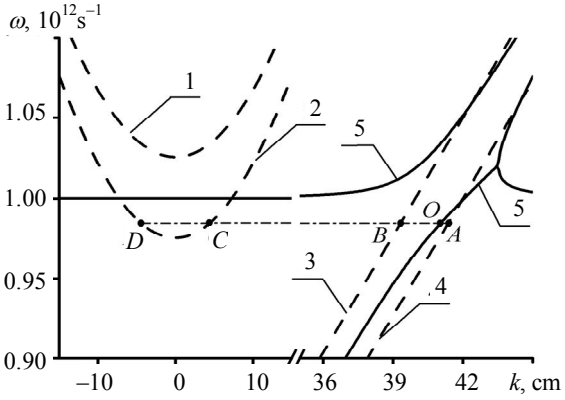

FIG. 2: Dispersion curves of electromagnetic signal waves (curves 1–4) and SCW (curves 5) in a PBSHFEL with the *H*-ubitron pumping and a non-axial electron beam injection. Beam injection angle is $\beta = 20°$

In this Figure the solid lines correspond to the dependence $\omega = \omega(k)$ for SCW (curves 5), the dashed lines – to the electromagnetic waves. The curve 1 corresponds to the ordinary electromagnetic wave, the curve 2 – to the extraordinary one, curves 3 and 4 correspond to the fast and slow cyclotron electromagnetic waves, respectively.

In order to obtain the maximum gain in PBSHFEL, the wave number k_3 and the frequency ω_3 of SCW were chosen to provide the maximum increment of SCW due to the plasma-beam instability.

It is known (e.g. from [2]) that this condition can be satisfied if the wave number is $k_3 = \omega_p / \upsilon_b$. This value of the wave number k_3 and the frequency ω_3 corresponds to the point O at the SCW dispersion curve (Fig. 2). According to the parametric resonance condition (1), the frequency of SCW and that of the electromagnetic signal should be the same: $\omega_1 = \omega_3$. Let us draw a horizontal line $\omega_1 = \omega_3 = \text{const}$ (dash-and-dot line AD) through the point O. Points A, B, C, D at the intersections of the line AD with dispersion curves of electromagnetic waves characterize the frequencies and the wave numbers of electromagnetic waves that can contribute to the parametric-resonance wave interaction in the considered system. Thus, there are four possible types of resonance wave interactions in this PBSHFEL which we denote as A, B, C, D

(according to the points *A*, *B*, *C*, *D* in Fig. 2). The key distinction of the considered model from that reported in paper [8], according to Fig. 2, is the proximity of the points *O* and *A*. These points can even coincide if the PBSHFEL parameters get slightly changed. Since the distance *OA* in Fig. 2 is numerically equal to the wave number k_2 of the magnetic pumping filed, the undulation period of the pump field in the mode *A* $\Lambda_A = 2\pi / k_2$ will be much longer than that in the modes *B*, *C* and *D*. If the point *O* and *A* coincide, the mode *A* has an additional resonance.

It should be noted that the cubic-nonlinear analysis of physical processes occurring in a PBSHFEL with the *H*-ubitron pumping and a non-axial beam injection has been performed only for the modes *C* and *D* [21], while modes *A* and *B* have not been analyzed before. These former modes are characterized by some conceptual features. First, these modes show the cyclotron instability, which is assumed to prompt the amplification rate. Second, the interaction between electrons in the beam and the electromagnetic wave is expected to be stronger, and the saturation level should be higher as well. These modes require more complex computations because of the cyclotron resonance: the electron rotation velocity in the magnetic field is approximately equal to the rotation velocity of the vector of signal's electric field strength. Thus, while using the average characteristics method for computation of these modes, we had to add a slow combination phase, whose time derivative is zeroed approximately:

$$\omega_1 - k_1 \overline{\upsilon}_{bz} + \eta_1 \omega_{H,b} / \overline{\gamma}_b \approx 0.$$

In this expression for a fast cyclotron wave we obtained $\eta_1 = +1$ (mode *B*), and for the slow one – $\eta_1 = -1$ (mode *A*).

For the PBSHFEL with the parameters listed above, the signal's wavelength in free space is 1.8 mm. By solving the set of equations (1), (9), (10), we easily find the undulator period of the magnetic pump field for each mode: Λ_A = 45.6 cm; Λ_B = 3.3 cm; Λ_C = 0.16 cm; Λ_D = 0.14 cm (the index corresponds to the interaction mode). Obviously, the most optimal mode in terms of implementation of a compact PBSHFEL is the *B-mode*. Modes *C* and *D* can be implemented with microundulators only. The *A* mode makes the system rather cumbersome.

Figure 3 presents the dependences between the first harmonics amplitudes of the electric field strength of the electromagnetic signal and the normalized time $\tau = t\delta\omega_0$ at various angles of beam injection in the interaction mode *B* (Fig. 2). The normalization factor $\delta\omega_0$ is equal to the increment of the plasma-beam instability, at the injection angle $\beta = 0°$.

According to Fig. 3, the saturation level grows as the beam injection angle β becomes larger, reaching its maximum at $\beta \approx 40°$. Note that the saturation level of the electromagnetic signal wave of ~ 5 MV/m is considered to be high enough. In the mode *A* the dependence between the saturation and the beam injection angle β is the same, but the saturation level in this case are much lower than in the mode *B*. As it was

mentioned above, the wave number of the magnetic pump field k_2 in Fig. 2 depends on the distance between points O and A. As this distance OA is the shortest among these four modes (OA, OB, OC, OD), the undulation period of the magnetic field in this mode proves to be the longest one $-\Lambda_A = 45.6$ cm. This fact seriously complicates the practical implementation of the mode A.

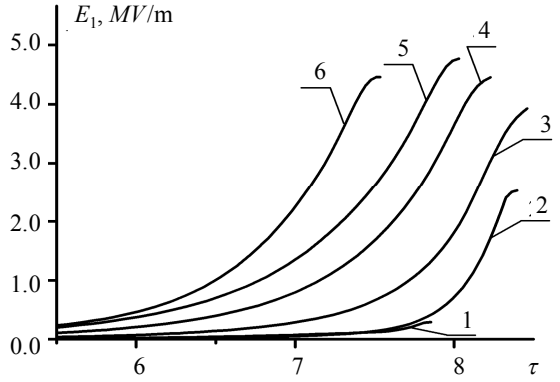

FIG. 3: Dependences of amplitudes of signal electric field strength on the normalized time $\tau = t\delta\omega_0$ at various angles of electron beam injection in the interaction mode B (Fig. 2). Curve 1 corresponds to $\beta = 0°$; curve 2 – $\beta = 10°$; curve 3 – $\beta = 20°$; curve 4 – $\beta = 30°$, curve 5 – $\beta = 40°$; curve 6 – $\beta = 50°$

It is also worth noting that the dependence between the saturation level and the beam injection angle β in the mode B differs fundamentally from that for the modes C and D. Thus, Fig. 4 shows the dependences between the amplitudes of signal's electric field strength and the normalized time $\tau = t\delta\omega_0$ at various beam injection angles in the interaction mode C (Fig. 2). Curve 1 corresponds to $\beta = 0°$, curve 2 – $\beta = 10°$, curve 3 – $\beta = 20°$ and curve 4 – to $\beta = 30°$.

It is obvious that in the mode C the maximum saturation level is reached at the axial beam injection $\beta = 0°$, while in the mode B the peak saturation is reached at the injection angle $\beta = 40°$. In the mode C, the saturation slightly decreases as the injection angle β grows, while in the mode B the saturation increases. The signal wave saturation in the mode C (Fig. 4) is almost twice as low as in the mode B. The amplitude dependences in the modes D and C are very similar. The relation between higher signal saturation levels at larger injection angles β in the mode B are associated with a stronger interaction between electromagnetic signal wave and electrons rotating in a longitudinal magnetic field. There is an evidence of the resonance interaction between the electromagnetic signal wave and a rotating electron beam.

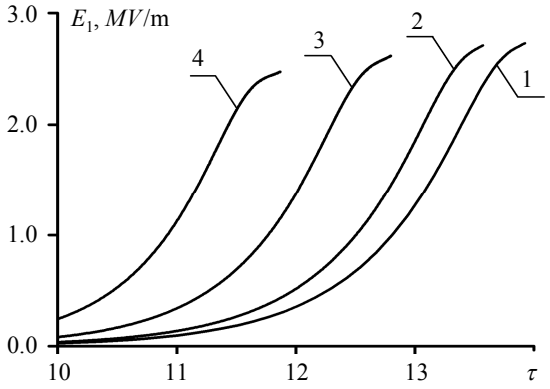

FIG. 4: Dependences of the amplitudes of signal electric field strength on the normalized time $\tau = t\delta\omega_0$ at various angles of electron beam injection in the interaction mode *C* (Fig. 2). Curve 1 corresponds to $\beta = 0°$; curve 2 – $\beta = 10°$; curve 3 – $\beta = 20°$; curve 4 – $\beta = 30°$

This interaction is the stronger, the higher the transverse velocity of the electron beam $\overline{\upsilon}_{b\perp}$, which in its turn is determined by the injection angle β. This results in an intensified pumping of energy from electrons in the beam to the electromagnetic wave. At the same time we observe the inverse process: the space-charge wave is suppressed by the electromagnetic wave. This is reflected in the fact that the SCW saturation level (Fig. 5) decreases as the beam injection angle β grows.

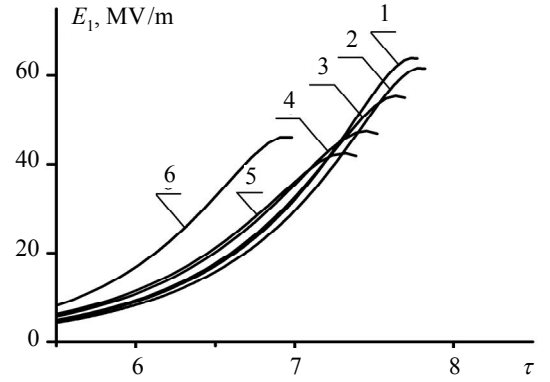

FIG. 5: Dependences of the amplitudes of SCW electric field strength on the normalized time $\tau = t\delta\omega_0$ at various angles of electron beam injection in the interaction mode *B* (Fig. 2). Curve 1 corresponds to $\beta = 0°$; curve 2 – $\beta = 10°$; curve 3 – $\beta = 20°$; curve 4 – $\beta = 30°$; curve 5 – $\beta = 40°$; curve 6 –$\beta = 50°$

The maximum suppression of SCW was registered at $\beta = 40°$ (curve 5 in Fig. 5). This angle is associated with the highest signal wave saturation (Fig. 3). Thus, due to

quite a strong parametric relation between SCW and the electromagnetic signal in the mode B, the SCW and the signal wave compete. This competition is the key factor that determines the saturation peak at the angle $\beta = 40°$.

The dependences of the amplitudes of SCW electric field strength on the normalized time at various angles of electron beam injection are different in the modes C and D (see, for example [21]). The SCW saturation level in these modes practically does not change at various injection angles. Here, the dynamics of the electromagnetic wave is determined by that of SCW.

According to plots in Fig. 3 and 5, the larger the angle β, the higher the amplification rate both for SCW (Fig. 5) and for the signal wave (Fig. 3). Such behavior is conditioned by the fact that at larger beam injection angles β the longitudinal velocity of electrons decreases, and longitudinal relativistic factor decreases, too

$$\gamma_{b\|} = \left(1 - \upsilon_b^2 \cos^2 \beta / c^2\right)^{-1/2},$$

hence, the increment of the plasma-beam instability grows [2,20].

5. CONCLUSIONS

The outcome of this study is a cubic-nonlinear theory of a plasma-beam superheterodyne free electron laser with the *H*-ubitron pumping for the case of a non-axial electron beam injection, which implements the parametric-resonance interaction between SCW and a cyclotron wave. This theory has to be taken into account the plasma-beam and cyclotron instabilities. It was revealed that the signal saturation for a mode utilizing a slow cyclotron wave (mode *B*), is much higher than in other modes (modes *A*, *C*, *D*). It was shown that in the considered device in the mode *B* the peak saturation of electromagnetic wave can be reached at the beam injection angle $\beta = 40°$. We found out that the maximum saturation can be reached due to the competition between SCW and the electromagnetic signal wave. In terms of practical implementation of a compact PBSHFEL, the interaction mode *B*, utilizing the magnetic pump field with the undulation period $\Lambda_B = 3.3$ cm, proved to be optimal. This mode allows generating a powerful electromagnetic signal wave having the electric field strength of about 5 MV/m in the millimeter wave range, while using a magnetic pump field with a relatively low magnetic field density (100 G). Thus there is every reason to believe that PBSHFELs operating at slow cyclotron waves are powerful sources of electromagnetic radiation in the millimeter wave range.

REFERENCES

1. Kulish, V.V., (2011), *Hierarchic electrodynamics and free electron lasers*, L.-N. Y.: Boca Raton, CRC Press, – 697 p.

2. Kuzelev, M.V., Rukhadze, A.A., and Strelkov, P.S., (2002), *Plasma relativistic microwave electronics*, Izd-vo MGTU, Moscow: 544 p. (in Russian).
3. Tsimring, S.E., (2007), *Electron beams and microwave vacuum electronics*, Hoboken, New Jersey: Wiley, – 573 p.
4. Booske, J.H., Dobbs, R.J., Joye, C.D. et al., (2011), Vacuum electronic high power terahertz sources, *IEEE Transactions on Terahertz Science and Technology*. **1**(1):54–75.
5. Kulish, V.V., Lysenko, A.V., and Brusnik, A.Ju., (2012), Hierarchical asymptotic methods in the theory of cluster free electron lasers, *J. Infrared Millimeter, Terahertz Waves*. **33**(2):149–173.
6. Kulish, V.V., Kuleshov, S.A., and Lysenko, A.V., (1993), Nonlinear self-consistent theory of superheterodyne and parametric electron laser, *J. Infrared Millimeter, Terahertz Waves*. **14**(3):451–567.
7. Kulish, V.V., Kuleshov, S.A., and Lysenko, A.V., (1994), Nonlinear self-consistent theory of two-stream superheterodyne free electron lasers, *J. Infrared Millimeter, Terahertz Waves*. **15**(1):77–120.
8. Kulish, V.V., Lysenko, A.V., and Koval, V.V., (2009), On the theory of a plasma-beam superheterodyne free electron laser with *H*-ubitron pumping, *Tech. Phys. Lett*. **35**(8):696–699.
9. Kulish, V.V., Lysenko, A.V., and Koval, V.V., (2010), Cubic-nonlinear theory of a plasma-beam superheterodyne free electron laser with *H*-ubitron pumping, *Telecommunications and Radio Engineering*. **69**(20):1859–1869.
10. Mohsenpour, T. and Amri, H.E., (2013), The gain equation of a helical wiggler free electron laser with ion-channel guiding and/or an axial magnetic field, *Chinese Phys. Lett*. **30**(3):34102–34105.
11. Sprangle, P., Granatstein, V.L., and Baker, L., (1975), Stimulated collective scattering from a magnetized relativistic electron beam, *Phys. Rev. A*. **12**(4):1697–1701.
12. Miroshnichenko, V.I., (1980), Forced coherent scattering of electromagnetic waves by a relativistic beam of oscillators, *Radiophys. and Quantum Electronics*. **23**(3):252–259 (in Russian).
13. Bekefi, G., (1992), Double-stream cyclotron maser, *Appl. Phys*. **71**(9):4128–4131.
14. Saviz, S., (2014), The effect of beam and plasma parameters on the four modes of plasma-loaded traveling-wave tube with tape helix, *J. Theoretical and Appl. Phys*. **8**(3):1–35.
15. Ginzburg, N.S. and Peskov, N.Yu., (2013), Nonlinear theory of a free electron laser with a helical wiggler and an axial guide magnetic field, *Phys. Rev. ST Accel. Beams*. **16**(9):090701.
16. Mohsenpour, T. and Mehrabi, N., (2013), Instability of wave modes in a two-stream free-electron laser with a helical wiggler and an axial magnetic field, *Physics of Plasmas*. **20**(8):082133 (7 p.).
17. Saviz, S., Rezaei, Z., and Aghamir, F.M., (2012), Gain enhancement in two-stream free electron laser with a planar wiggler and an axial guide magnetic field, *Chin. Phys. B*. **21**(9):094103 (4 p.).
18. Liu, W., Yang, Z., Liang, Z., (2006), Instability of two-stream free-electron laser with an axial guiding magnetic field, *J. Infrared Millimeter, Terahertz Waves*. **27**(8):1073–1085.
19. Meydanloo, S. and Saviz, S., (2014), Dispersion relation and growth rate in two-stream thermal plasma-loaded free-electron laser with helical wiggler, *J. Theoretical and Appl. Phys*. **9**(1):39–43.
20. Kulish, V.V., Lysenko, A.V., Oleksiienko, G.A. et al., (2014), Plasma-beam superheterodyne FELs with helical electron beams, *Prikladnaja Fizika*, 5:24–28 (in Russian).
21. Lysenko, A.V., Alekseyenko, G.A., and Fedenko, M.O., Application of an upgraded method of averaged characteristics to the problems of theory of plasma-beam superheterodyne free electron laser, *Zh. Nano- i Elektr. Fiz*., **7**(4):04083(8 p) (in Russian).